

Persistence Terrace for Topological Inference of Point Cloud Data

Chul Moon^{*1}, Noah Giansiracusa^{†2}, and Nicole Lazar¹

¹University of Georgia

²Swarthmore College

February 28, 2023

Abstract

Topological data analysis (TDA) is a rapidly developing collection of methods for studying the shape of point cloud and other data types. One popular approach, designed to be robust to noise and outliers, is to first use a nearest neighbor function to smooth the point cloud into a manifold and then apply persistent homology to a Morse filtration. A significant challenge is that this smoothing process involves the choice of a parameter and persistent homology is highly sensitive to that choice; moreover, important scale information is lost. We propose a novel topological summary plot, called a persistence terrace, that incorporates a wide range of smoothing parameters and is robust, multi-scale, and parameter-free. This plot allows one to isolate distinct topological signals that may have merged for any fixed value of the smoothing parameter, and it also allows one to infer the size and point density of each topological feature. We illustrate our method in some simple settings where noise is a serious issue for previous TDA frameworks and then we apply it to a real data set by counting muscle fibers in a cross-sectional image.

Keywords: topological data analysis; point cloud; persistent homology; density estimation; Morse theory.

^{*}Supported in part by NSF IIS-1607919.

[†]Supported in part by NSA grant H98230-16-1-0015.

1 Introduction

A defining characteristic of many modern data applications – whether they fall under the heading of “Big Data” or not – is their unstructured nature. It can no longer be assumed that data will come to us for analysis in regular arrays with fixed numbers of rows and columns and a single observation in each cell, usually representing the measured value of a particular variable for a particular unit. Similarly, questions of scientific interest have been shifting in recent years. In settings such as neuroimaging and genetics, to give two prominent examples, researchers are focusing on questions about network structure, interactions between brain regions or regions on the genome, and the like. Such questions are not amenable to traditional statistical procedures based on simple array-structured data. Accordingly, recent years have seen the development of methods for functional (Ramsay and Silverman, 2005), object-oriented (Marron and Alonso, 2014), and symbolic (Billard and Diday, 2007) data. All of these aim to tackle situations where the basic unit of analysis is something other than a traditional observation; rather, it can now be an entire image, or a histogram, or a function.

A relatively new, emergent approach is topological data analysis (TDA), which focuses on the “shape” of a data set (Carlsson, 2009; Lum et al., 2013). A popular source of data for successful applications of TDA has been biology; examples include the study of brain artery structure (Bendich et al., 2016); brain networks (Lee et al., 2012; Petri et al., 2014); protein structure (Gameiro et al., 2015); viral genomics (Chan et al., 2013); bone structures (Heo et al., 2012; Turner et al., 2014); and breast cancer (Nicolau et al., 2011).

A prominent branch of TDA is persistent homology, which analyzes the dynamics of the topological features of a data set. Features are defined through a filtration; as the filtration value changes, topological features are “born” (appear) and “die” (disappear). A major challenge in the TDA approach is to decide which features are real, in the sense of representing meaningful structure in the data, and which are artifacts of the noise inherent in all measured data. This is a question of statistical inference, and as such, recent years have seen the development of statistical methods to blend with the topological concepts underlying persistent homology. Fasy et al. (2014) determine significant features using a confidence set for the persistence diagram, which summarizes the persistent homology of a

data set. Another confidence set approach (Chazal et al., 2015) is based on the persistence landscape, an alternative summary of persistent homology information (Bubenik, 2015).

Persistent homology results are sensitive to noise and outliers in the data, hence robust smoothing-based approaches have also been proposed. Some works in this direction include Bobrowski et al. (2017), Bubenik (2015), and Phillips et al. (2013). However, smoothing to make a more robust procedure is not without drawbacks. First, there might not be a single optimal value of the smoothing parameter, since persistent homology simultaneously tracks topological features appearing in the data at different scales. Second, the smoothing operation emphasizes point density and thereby loses important information about the size of topological features in the data.

In this paper we suggest a new summary plot that we call the “persistence terrace,” due to its three-dimensional staircase structure, that aims to rectify the two disadvantages of smoothing in this context. The persistence terrace incorporates multiple filtration values (which allows one to keep track of the births and deaths of topological features.) *and* multiple smoothing parameter values (which removes the need to pick a single smoothing parameter to represent all features), thereby revealing the topological interaction between these two parameters. In doing so, the persistence terrace helps to distinguish statistical signals that may be overlooked by currently existing methods; moreover, it simultaneously reflects both the size and density of topological features in the data. Learning how to interpret the persistence terrace does take practice, so we illustrate our methods on both simulated and real data and offer insight into the meaning of different terrace features, shapes, and sizes.

The rest of paper is organized as follows. In Section 2 we provide mathematical background, then review the standard persistent homology framework; we also discuss limitations when applying it to data analysis. Section 3 introduces the persistence terrace and demonstrates its important characteristics with simple examples. In Section 4 we explore the persistence terrace on more complex simulated and real data. Finally, in Section 5 we discuss our main findings and give directions for future work.

2 Persistent Homology in TDA

This section summarizes the theoretical background of (persistent) homology (Hatcher, 2002; Edelsbrunner and Harer, 2008, 2010; Ghrist, 2008; Zomorodian, 2012) and discusses some statistical short-comings when applied to data analysis.

2.1 Homology and Simplicial Complexes

A topological space is a mathematical object abstracting the intuitive notions of nearness, connectivity, and continuity. Any metric space (such as \mathbb{R}^n), or subset thereof, can be viewed as a topological space. Homology is used to quantify the topological characteristics of a topological space. The dimension of the k th homology vector space is called the k th Betti number, and it counts the number of k -dimensional holes in the space. Table 1 gives the geometric interpretations of the $k = 0, 1, 2$ Betti numbers.

Symbol	Dimension	Counts
β_0	0	Number of connected components
β_1	1	Number of loops
β_2	2	Number of enclosed solid voids

Table 1: Betti numbers.

Figure 1 illustrates the Betti numbers of a point, circle, and torus (hollow donut). Each has a single connected component; the circle has a single loop; the torus has two loops (in the vertical and horizontal directions) and encloses a single solid void.

In order to perform computations on a topological space, one needs to discretize and represent the space with a finite amount of information. Fortunately, this is possible for most spaces appearing in practice through the process of triangulation: we encode the space as a *simplicial complex*, which means a collection of vertices, edges, triangles, tetrahedra, and higher-dimensional simplices, together with the data of how all these pieces are attached. For instance, the circle is a single vertex with a single edge attached at both ends to the vertex; if we add a diagonal edge to each rectangular region of the torus depicted in Figure 1 then we have decomposed the torus into a collection of attached triangles. The

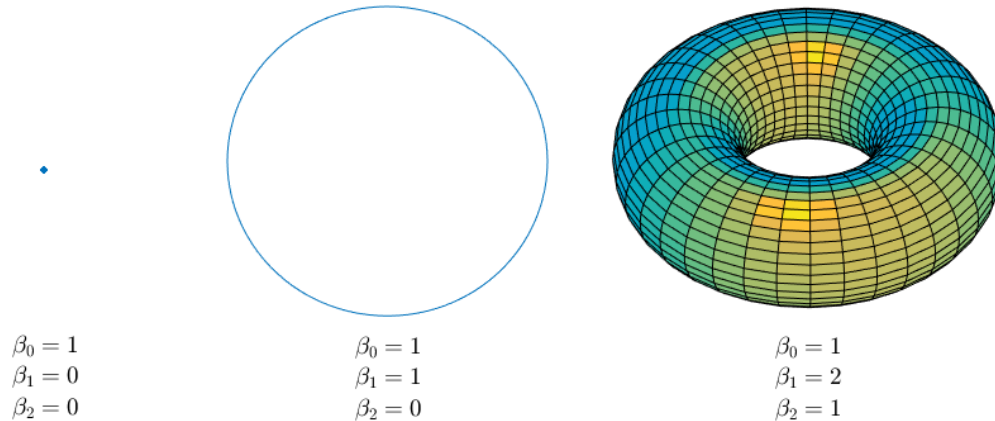


Figure 1: Betti numbers of a point (left), a circle (center), and a torus (right).

computation of Betti numbers from a simplicial complex representation of a topological space is standard linear algebra and in particular is quite efficient, algorithmically speaking.

2.2 Persistent Homology

For a 1-parameter family of topological spaces, or simplicial complexes, *persistent homology* offers a method of quantifying the dynamics of topological features (e.g., when holes appear and disappear). A 1-parameter family of simplicial complexes where simplices are added but never removed is called a *filtered* simplicial complex, and the parameter is then usually called a *filtration* parameter.

A *point cloud*—a finite, unordered collection of points in \mathbb{R}^n or some other metric space—is uninteresting as a topological space since it is discrete: β_0 is the number of points in the cloud and $\beta_k = 0$ for all $k \geq 1$. However, TDA introduces methods of building a filtered simplicial complex from a point cloud, thereby reconstructing multi-scale topological features of the object or distribution from which the points are sampled. The standard approach is called the *Rips* complex: the points in the cloud serve as the vertices; pairs of points are joined by an edge when their distance is less than the filtration value; all possible higher-dimensional simplices are filled in (that is, whenever three points are connected by all three possible edges, a triangle is filled in, and whenever four points are joined by all six possible edges, a tetrahedron is filled in, etc.).

Persistent homology can be visually summarized with *barcodes*: for each k , plot a collection of horizontal intervals whose left endpoint is the filtration value at which a particular k -dimensional homology class is born and whose right endpoint indicates its death. The number of intervals over a filtration value is the Betti number β_k at that value. A more compact visual summary is the *persistence diagram*: here each homology class is plotted as a point whose x -coordinate is the birth time and y -coordinate is the death time; different symbols are used to distinguish homological dimension. The prominence, or persistence, of a topological feature corresponds to the length of a bar in a barcode, or to the height above the diagonal line $y = x$ in a persistence diagram.

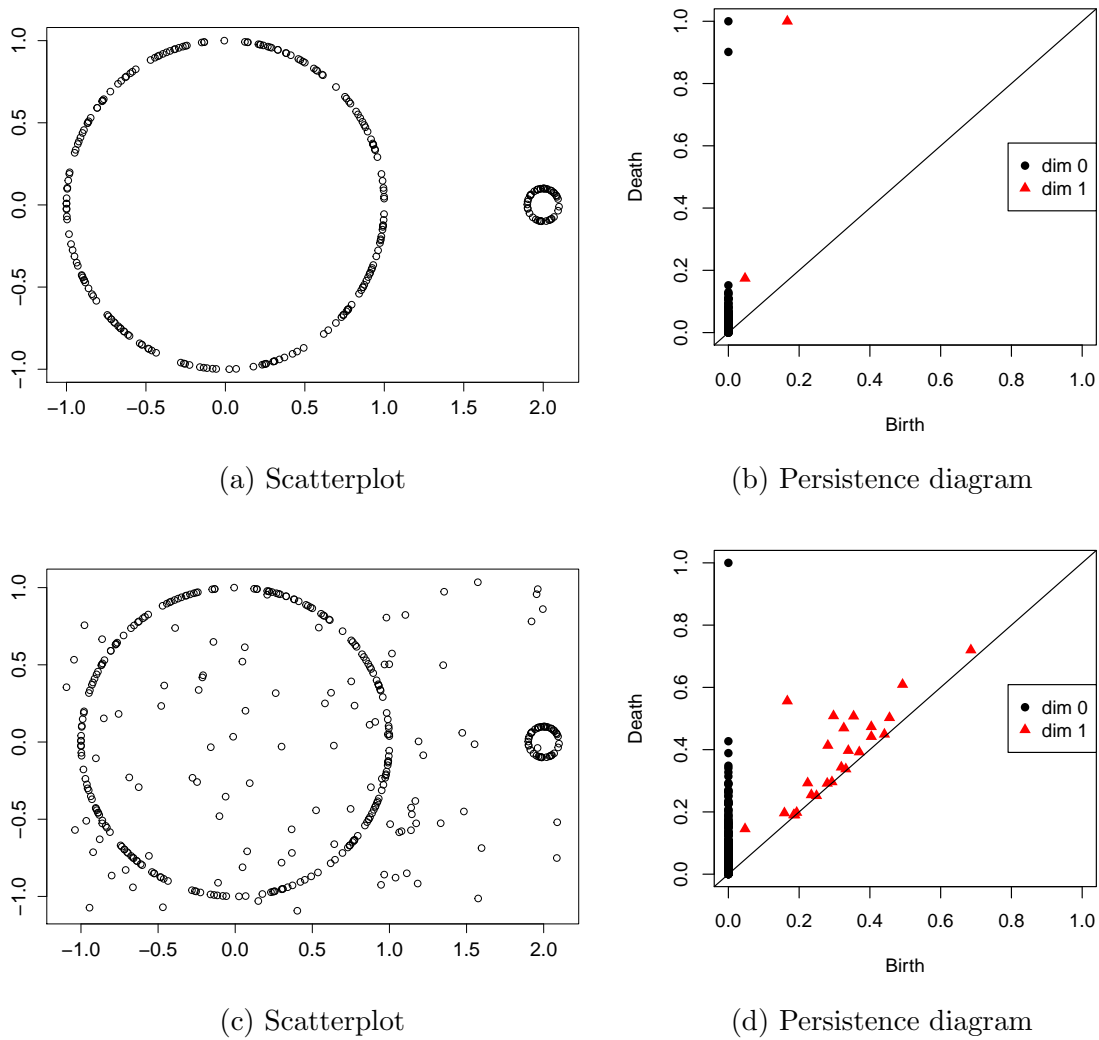


Figure 2: Scatterplots and persistence diagrams for points concentrating around two circles.

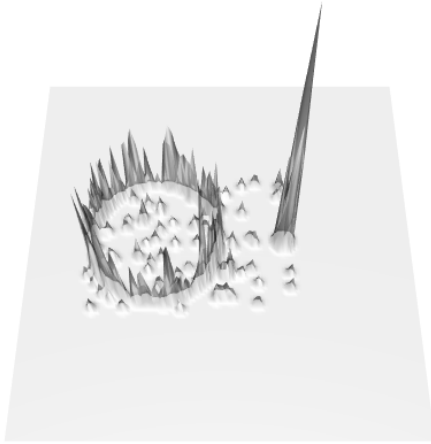
Figure 2 shows point cloud scatterplots and the persistence diagrams obtained using the Rips complex. Note that when there is no noise, the persistence of a dimension one feature (triangle plotted above the diagonal) is heavily affected by the radius of the circle it comes from; when noise is added, many false loops appear in the persistence diagram and it becomes difficult to infer the number of actual circles in the point cloud.

2.3 Robust Morse-Based Approach

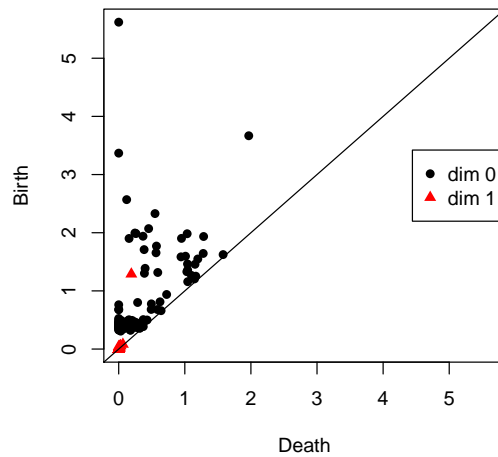
To overcome sensitivity to noise and outliers, robust TDA approaches have been developed using distance-to-measure functions (Chazal et al., 2011), kernel distances (Phillips et al., 2013), kernel density estimators (Fasy et al., 2014), and kernel estimations (Bobrowski et al., 2017). These methods first transform a discrete point cloud into a continuous *manifold* via a smoothing function. For example, graphing the m th nearest neighbor function turns a point cloud in \mathbb{R}^2 into a surface in \mathbb{R}^3 ; the larger the value of m , the more rounded this surface will be. The manifold thus obtained can be filtered by its super-level sets, sets above a threshold value. The filtered super-level sets yield a 1-parameter family of topological spaces—which, when triangulated for computational purposes, is a filtered simplicial complex called the *Morse complex* of the point cloud—so once again persistent homology can be computed. The Morse complex is constructed with the smoothing function; the resulting persistent homology is more robust than that of the Rips complex.

There are disadvantages to these robust Morse-based smoothing approaches. First, it is difficult to find a single optimal smoothing parameter such that the corresponding persistent homology reveals features occurring at different scales. For example, in Figure 3 we use the “two noisy circles” data from Figure 2c and apply the kernel density estimator with two different smoothing parameter values. From the persistence diagrams, we see that the noise has been cleaned up by switching from the Rips complex to the Morse complex—but for both smoothing parameter values, one of the two actual circles has been washed away in the process.

A second issue is that the Morse filtration only computes the number of k -dimensional holes of the level sets, not their sizes, so important scale information is lost. Figure 4 shows a point cloud with three circles, each containing 200 points. The Morse persistence



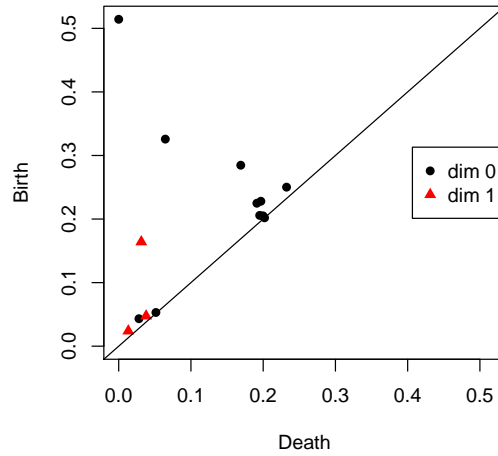
(a) Manifold at smoothing parameter 0.03



(b) Persistence diagram at smoothing 0.03



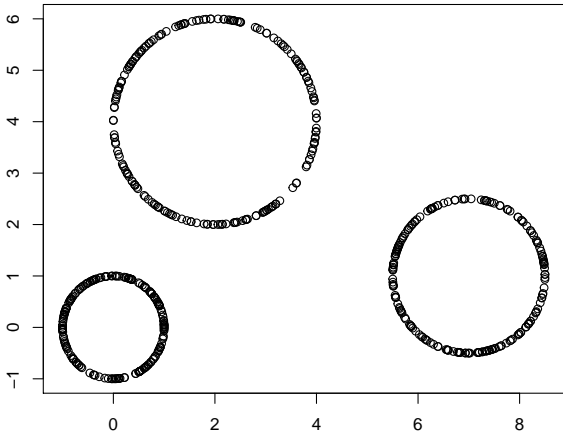
(c) Manifold at smoothing parameter 0.2



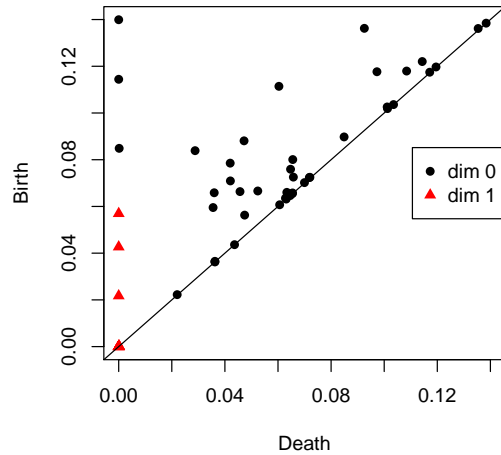
(d) Persistence diagram at smoothing 0.2

Figure 3: Manifolds and persistence diagrams for two noisy circles data.

diagram indicates three prominent loops in the data, but the height of each triangle above the diagonal line positively relates to the density of points on the corresponding circle and thus is negatively related to the radius. By decreasing the density of the smallest circle to match that of the largest circle, we would see the top triangle in the persistence diagram fall down to the height of what is presently the third triangle.



(a) Scatterplot



(b) Persistence diagram of Morse filtration

Figure 4: Point cloud and persistence diagram for three circles.

2.4 Significance of Features

The significance of a topological feature is generally recognized by the height-above-diagonal of a point in a persistence diagram. Despite important steps toward a rigorous statistical theory of quantifying significance and producing confidence interval type analysis for persistent homology (Fasy et al., 2014; Chazal et al., 2014; Chazal et al., 2015), serious conceptual challenges remain.

In a Rips complex, a small feature with high density is usually seen as insignificant because the Rips complex fills in the hole so quickly. On the other hand, for the robust Morse-based approach, the significance depends, in addition to height-above-diagonal, on the smoothing parameter. The smoothing parameter is chosen based on the size of data features one aims to uncover, but then height-above-diagonal in the persistence diagram reflects the density of points more than their significance. Therefore, whether using Rips or Morse, it is impossible to fully capture significance with a single diagram: the significance of a feature depends on both its *size* and *density*. In the following section, we introduce the persistence terrace which is robust to noise and simultaneously reveals significance with regard to both size and point density of each topological feature.

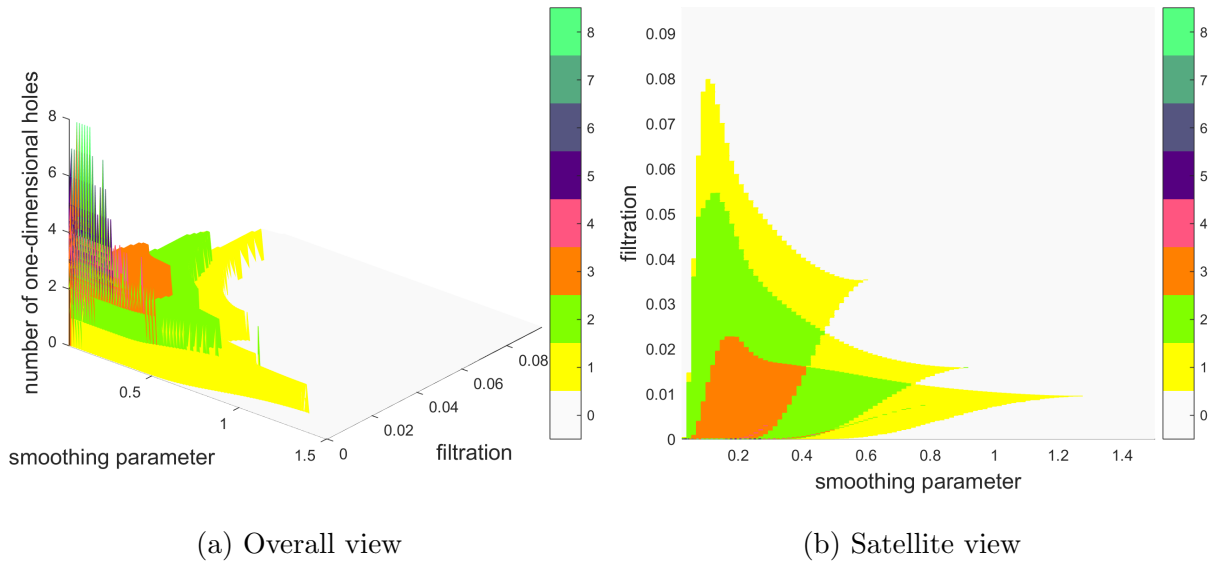


Figure 5: Dimension one persistence terrace for three circles data.

3 Persistence Terrace

The persistence terrace uses robust Morse-based persistent homology, but by incorporating a range of smoothing parameters it provides a more detailed summary of topological features. For each dimension k , we plot a surface where the x -axis is the smoothing parameter, the y -axis is the filtration value, and the z -axis is the Betti number β_k . Thus, for a point cloud in \mathbb{R}^n , a point on the persistence terrace with coordinates (x_0, y_0, z_0) means there are z_0 holes of dimension k on the Euclidean subset

$$\{\vec{v} \in \mathbb{R}^n \mid f_{x_0}(\vec{v}) \geq y_0\},$$

where $f_{x_0} : \mathbb{R}^n \rightarrow \mathbb{R}$ is the chosen smoothing function corresponding to parameter x_0 . Note that this subset is topologically equivalent to its graph in \mathbb{R}^{n+1} under the function f_{x_0} , which is the super-level set used in Morse-based persistent homology.

Because Betti numbers are always integers, and they tend not to have gaps when the two parameters (smoothing and filtration) are varied by small amounts, the surfaces plotted in a persistence terrace consist of flat layers that somewhat resemble a rice terrace (see Figure 5a). Each k -dimensional topological feature in the point cloud contributes a layer to the persistence terrace; when there is a range of parameters for which multiple features are detectable, the corresponding layers in the terrace stack on top of each other and

result in a higher altitude layer over their intersection. Thus, when there is an “optimal” range for both parameters, the persistence terrace readily shows a region where all layers simultaneously overlap; the number of distinct k -dimensional holes is then simply the height of the terrace at this region of maximal overlap. This is the case in Figure 5, where we use the three circles point cloud from Figure 4a and set $k = 1$ to detect loops in the data. Near the origin there are lots of spikes resulting from noise, but this quickly settles down and the three distinct loops are easily seen (the large regions of height one), as well as their regions of double overlap (height two) and the optimal region of triple overlap (height three) correctly indicating three loops in the data.

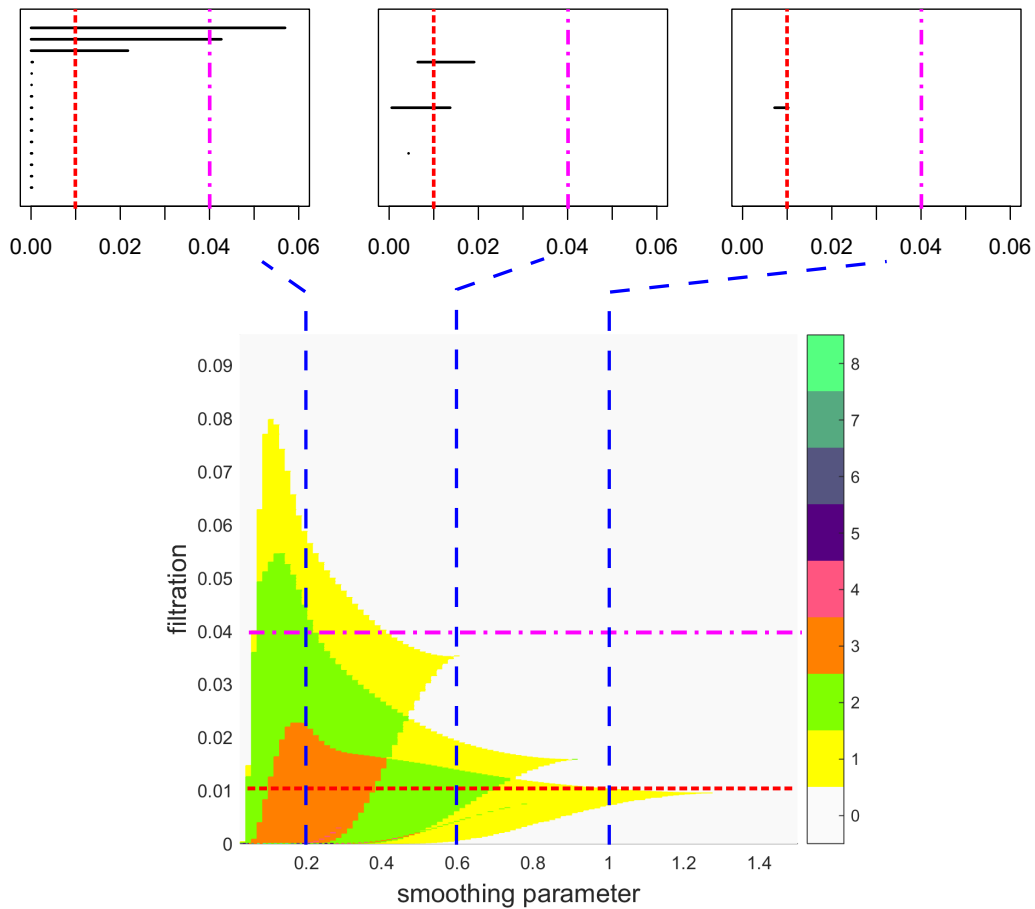


Figure 6: Barcodes corresponding to vertical slices of the persistence terrace.

The relationship between the persistence terrace and traditional TDA barcodes is illustrated in Figure 6. Fixing a value of the smoothing parameter corresponds to taking a

vertical slice of the persistence terrace. While this slice of the terrace shows the Betti number β_k at each filtration value, the barcode indicates this Betti number with β_k separate horizontal intervals. In Figure 6 we have chosen three different values of the smoothing parameter at which to slice the terrace and draw the corresponding barcode; since barcodes traditionally use the filtration value for the x -axis, one needs to mentally rotate the barcode counterclockwise 90 degrees to match up with the y -axis of the terrace.

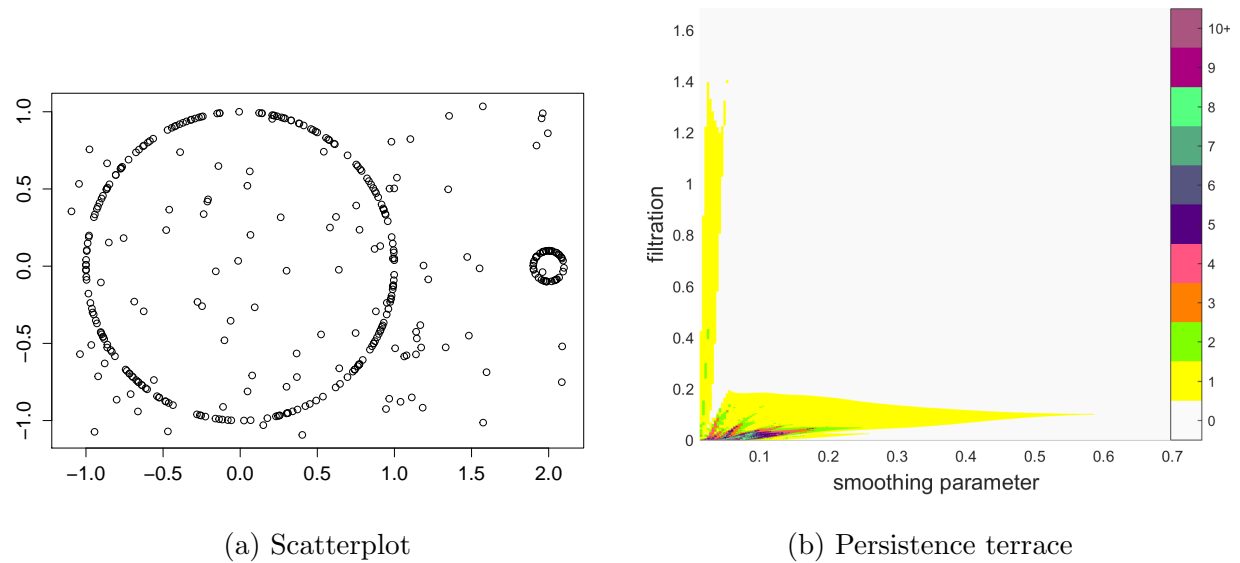


Figure 7: Noise-added two circle data and dimension one persistence terrace.

The persistence terrace allows us to visually separate out the different layers and hence count topological features even when there is no value of the smoothing parameter that could be used to detect all features. Recall that in Figure 3 we tried two different values of the smoothing parameter, and in each case lost the information of one of the two circles. This suggests that there is no optimal smoothing parameter. Nonetheless, the persistence terrace in Figure 7b shows two clear, distinct height one layers (one vertically oriented, one horizontally oriented), where any optimal range of smoothing parameter is so small it is essentially impossible to locate. Therefore, one readily infers two distinct loops in the data even though the standard Rips approach fails due to noise and the robust Morse approaches fail due to inadequacies of smoothing.

Moreover, the shape and location of these two layers in the terrace are determined by—and hence speak to—the size and density of the circles in the point cloud. The vertical

layer in the terrace comes from the small, dense circle since it survives only for small values of the smoothing parameter before it becomes filled in; the horizontal layer comes from the large circle, since it survives only for small values of the filtration parameter due to lower density, hence lower altitude, of the corresponding manifolds (cf., again, Figure 3). More generally, the horizontal width of a terrace layer is positively related to the size of the corresponding feature in the data and the vertical length with the density of points on the feature. Thus, from the persistence terrace alone in Figure 7b we would correctly infer that our data consist of two circles, one large and the other smaller and denser.

3.1 Computational algorithm

The computation of a persistence terrace can be divided into three algorithmic steps:

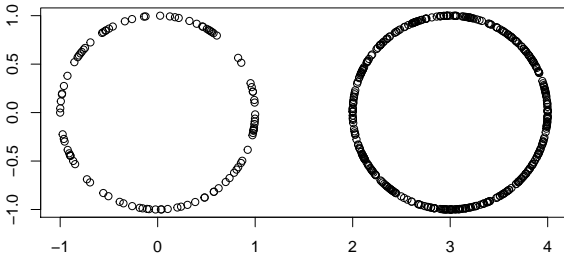
$$\text{Point cloud data} \xrightarrow{\text{Step 1}} \text{Barcodes} \xrightarrow{\text{Step 2}} \text{Betti numbers} \xrightarrow{\text{Step 3}} \text{Persistence terrace}$$

First, we compute the barcodes for the Morse complexes corresponding to a pre-defined vector of smoothing parameter values, using a specified smoothing function. This is accomplished using a simple “for loop” and any of the pre-existing persistent homology software packages that includes Morse complex barcodes. We use the R package TDA (Fasy et al., 2016) for this step. Second (Algorithm 1 in Supplementary Material), we fix a dimension k and for each fixed value of the smoothing parameter compute the Betti number β_k using the k -dimensional barcodes. Third (Algorithm 2 in Supplementary Material), use the fact that for each fixed smoothing parameter value the function β_k just computed is a step function, only changing value at the filtration values computed in the previous step, in order to assemble all the Betti numbers into the persistence terrace. We plot a persistence terrace using Matlab (MATLAB, 2016).

Note that, while producing a persistence terrace is fairly computationally intensive, it is readily parallelizable since all the computations for a fixed value of the smoothing parameter are independent of the computations for the others.

3.2 Detection of Features with Different Densities

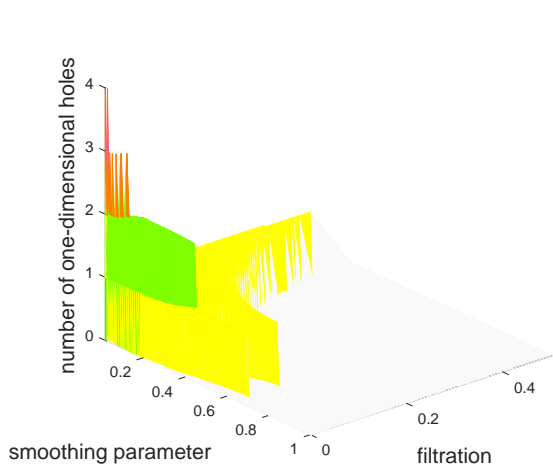
We can use the persistence terrace to identify differences in the densities of data points that make up the various topological features in the point cloud. As discussed earlier, the persistence terrace can often be visually decomposed into height one layers that overlap with each other in various regions. The length of each height one layer along the y -axis (i.e., the range of filtration values for which the corresponding topological feature persists) positively relates to the density of points in that feature. Indeed, high density means that the smoothing function will take large values, so the manifold it produces will be very tall over high density regions and consequently that portion of its level set topology will remain constant for a large range of filtration values.



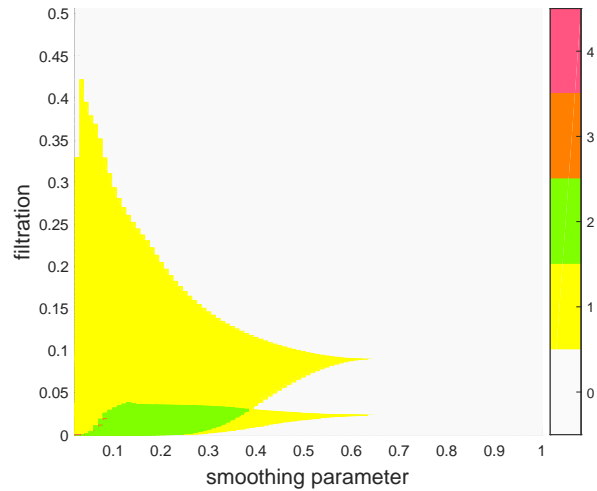
(a) Scatterplot



(b) Manifold from smoothing parameter 0.2



(c) Persistence terrace for β_1



(d) Satellite view

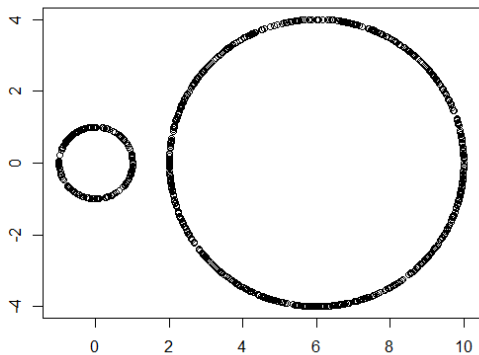
Figure 8: The high density circle smooths to a high altitude volcano and appears as a persistence terrace layer stretching along a wide stretch of the y -axis in the satellite view.

To illustrate this, we generate 100 and 400 random points from two equal sized circles. Figure 9b shows how the higher point density of the second circle is manifest as a higher altitude volcano-shaped manifold after smoothing (here with a Gaussian kernel density estimator with parameter $h = 0.2$). In the β_1 persistence terrace we see two height one terrace layers with a clear region of height two overlap. Looking at the satellite view of the persistence terrace, we see that both layers reach horizontally to equal maximal values of the smoothing parameter (which, as we discuss in the next subsection, stems from the fact that the circles have the same radius), but one layer reaches much further vertically along the filtration axis. This taller terrace layer represents the denser circle, since for large values of the filtration parameter the super-level set of the tall volcano will be an annulus (which, topologically, is a circle) while that of the short volcano will be empty. If we were to remove the dense circle from the point cloud and re-plot the persistence terrace, we would see this tall terrace removed (so the height two overlap would drop down to height one) and the shorter terrace layer would remain unchanged. Thus the two topological signals have been completely disentangled and identified by their corresponding point densities.

3.3 Detection of Features with Different Sizes

We can also infer the size of topological features in a point cloud from the persistence terrace. Just as density was measured by how far a terrace layer stretches along the y -axis in the satellite view, size is measured by how far it stretches along the x -axis, by the range of smoothing parameters for which the corresponding feature is detectable. Indeed, as the smoothing parameter increases, the corresponding manifolds become more rounded so the finer topological features of the super-level sets get washed away.

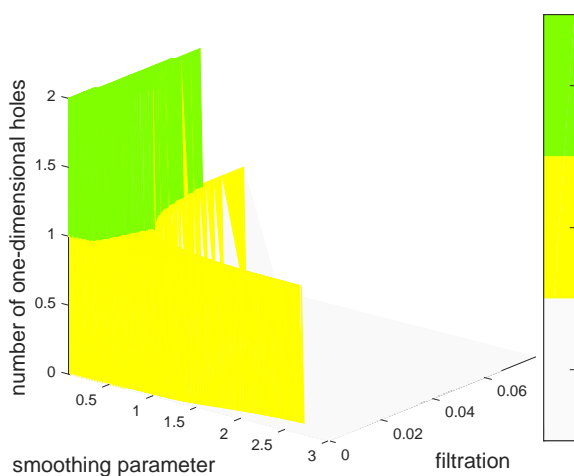
To illustrate this, we generate 200 points on a radius 1 circle and 800 points on a radius 4 circle. The two circles have almost the same point densities. We see in Figure 9b that they smooth into volcanoes of similar height. The β_1 persistence terrace clearly consists of two overlapping height one layers. As expected, these layers reach to roughly comparable heights along the y -axis since the two densities agree, but one terrace layer reaches much further along the x -axis: the volcano coming from the smaller circle fills in more quickly than that of the larger circle as the smoothing parameter is increased.



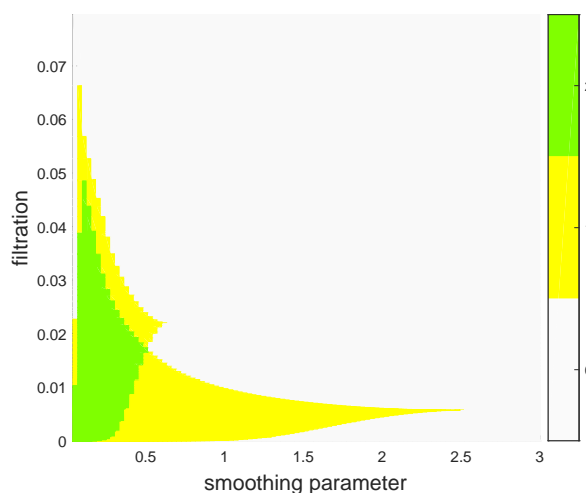
(a) Scatterplot



(b) Smoothed manifold



(c) Persistence terrace for β_1



(d) Satellite view

Figure 9: Two circles with equal density but unequal radius. The volcano manifold from the small circle fills in more quickly as the smoothing parameter is increased.

4 Simulation Study

The data sets in the previous section are deliberately very simple in order to focus the discussion and analysis of persistence terraces on specific attributes and behaviors. In this section we explore two data sets that are less artificial: one involves different shapes and more noise/distortions, the other comes from medical imaging.

4.1 Features with Stochastic Noise

Here we demonstrate that the persistence terrace can be used to help analyze data that are both noisy and less uniform than in the previous section. We generate a stochastic planar point cloud with points clustering around four “holes”, so that four topological loops should be present (see Figure 10a). Specifically, we create a radius 1 circle with 800 points in total. For inside and outside of the circle, 400 points are generated that follow an exponential distribution with rate 4 and 10, respectively. We place 400 points uniformly randomly on a 1×1 square then perturb these points with random $N(0, 0.15)$ noise. We also create an equilateral and an isosceles triangle, by placing 200 points randomly uniformly on each triangle edge, but then perturb these points with $N(0, 0.15)$ noise. The persistence diagram in Figure 10b is computed using the Rips complex. While some triangles in that diagram are far above the diagonal line, suggesting persistent loops in the data, there is far too much noise to be able to infer the correct number of loops, namely $\beta_1 = 4$.

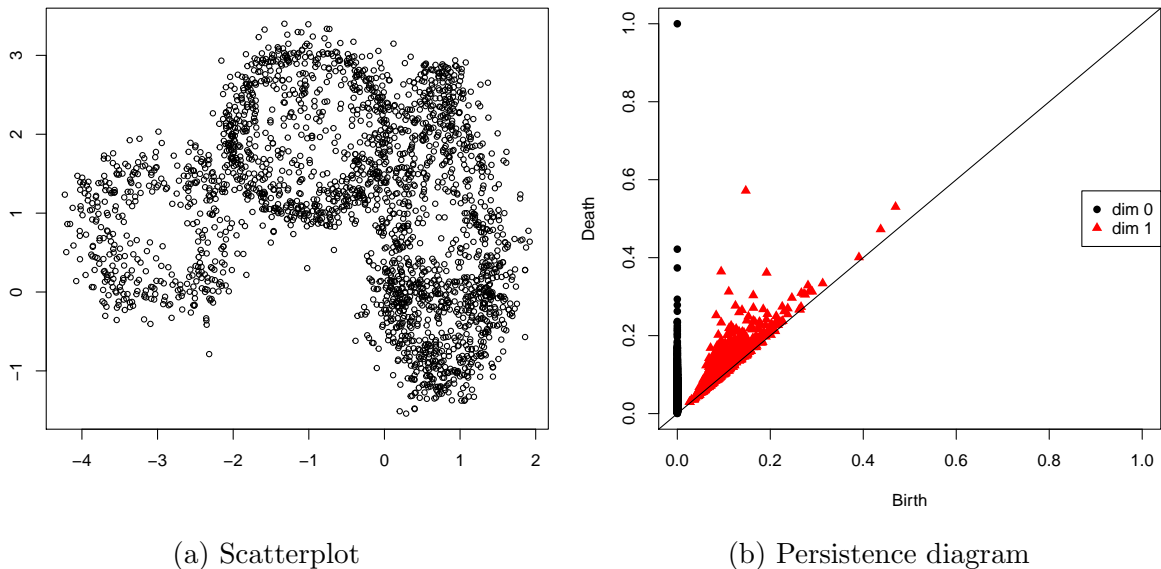


Figure 10: Point cloud of four noisy shapes and the Rips persistence diagram.

In Figure 11 we plot the one-dimensional persistence terrace using the kernel density estimator with 100 smoothing parameter values evenly distributed between 0.01 to 0.6. The terrace detects up to 152 loops in the data, though most of these only occur for relatively small values of the smoothing parameter. Since we expect very large values of β_1 to be

considered noise, we put all levels greater than 10 into a single category.

When ignoring the “noisy region” where these high levels occur, and the regions immediately surrounding it, we observe that there are three height one triangular layers stretching to the right in the satellite view of the persistence terrace. This suggests we have found all but one of the loops we hoped to find in the point cloud. However, there is actually a fourth prominent layer clearly visible, it is simply contained entirely within the largest of the height one layers: this fourth layer is the height two region stretching rightward to just under smoothing parameter 0.4. The height three layer also seen is then easily deduced to be an intersection of three already accounted for layers and so should not be counted as an additional feature. Thus, with proper attention to overlap, we do in fact count precisely four prominent terrace layers.

By contrast, the Rips persistence diagram was unable to achieve this correct count. Since there is no prominent height four region in the terrace (the four layers we identified never overlap simultaneously), it follows that there is no single smoothing parameter that would yield the correct number of loops. Thus relying on Rips or any individual Morse persistence diagram would result in an incorrect loop count. We need the persistence terrace to properly disentangle and count the topological signals in this noisy point cloud.

In addition, we can use the methods from the previous section to give a rough, qualitative description of the four loops in the data identified by the persistence terrace. The two largest loops have roughly the same size though one has slightly greater point density; this latter density matches the density of another, slightly smaller loop; finally, the fourth loop is both smaller and denser than the rest. This description appears to accord with the square, circle, isosceles triangle, and equilateral triangle, respectively.

4.2 Counting Muscle Fibers

Muscle tissue consists of tube-like shapes known as muscle fibers which are bundles of filaments ensheathed by a connective tissue known as endomysium. A cross-section of a muscle thus reveals a collection of semi-homogeneous regions (if one blurs the filaments together), one for each muscle fiber, that are delineated by walls made of endomysium. Counting the number of muscle fibers in a cross-sectional slice of a tissue sample can therefore be viewed

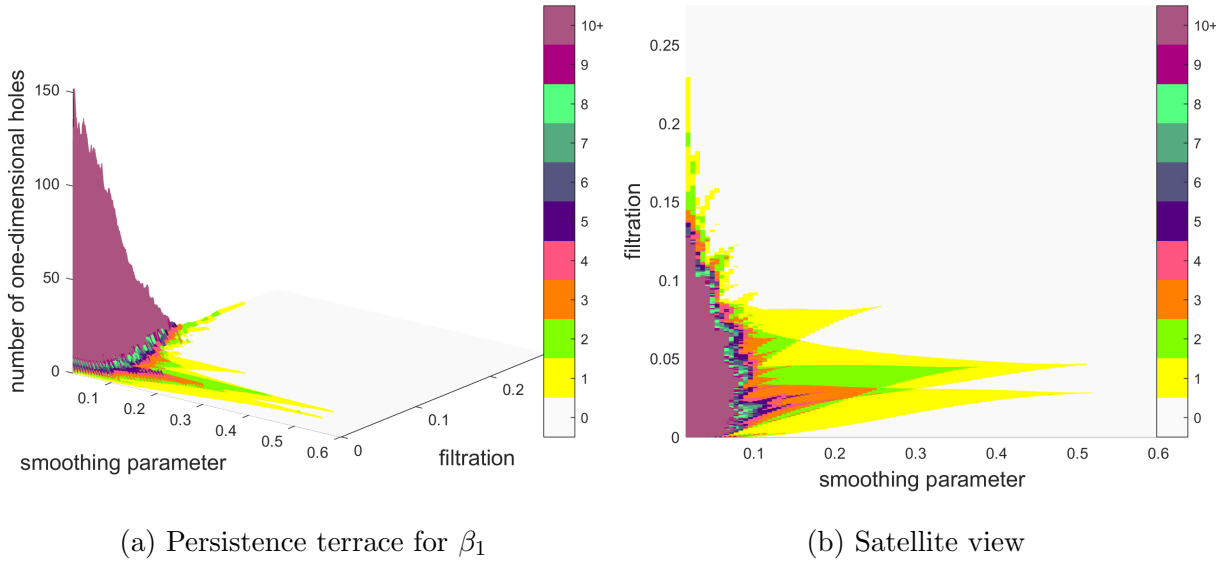


Figure 11: The β_1 persistence terrace for the noisy four shape point cloud. There are four prominent layers, corresponding to the four data loops, though one is stacked on another.

as a topological problem: we need to compute the number of independent loops formed by the endomysium. Since the sizes of the loops vary and the cross-sectional image is bound to have noise, this is a natural setting to apply the persistence terrace. For this example, we adapt Figure 1 of Mula et al. (2013), the muscle tissue cross-sectional image.

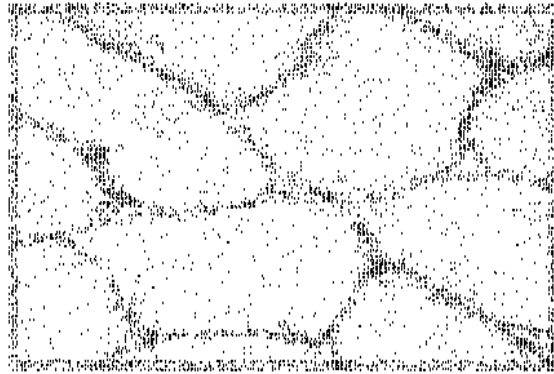


Figure 12: Scatterplot of points sampled from the muscle tissue cross-sectional image.

The first step in applying the persistence terrace method is to convert the cross-sectional image into a point cloud. Since we are interested in the loops made from the endomysium, we should sample points from the endomysium in the cross-sectional image. To do this, we first convert the original image to a grayscale intensity image. Next, we randomly

select 5,000 endomysial points from the grayscale image. We sample in proportion to the grayscale intensity so that darker pixels have a higher likelihood to be selected. Since the cross-sectional image contains several incomplete muscle fibers at the boundary that we would like to include in the count, we add lines around the boundary of the black-and-white image to artificially close off all the broken loops. For the particular cross-sectional image we are using here, this results in 11 muscle fibers, including these partial boundary fibers. We generate an additional 1,500 points by randomly sampling from the boundary. The resulting point cloud is shown in Figure 12.

Note that the muscle fiber cross-sections vary considerably in size, shape, and convexity. Note also that there are two types of noise: black pixels within the muscle fibers and white pixels within the endomysium, both due to sampling error. There is a further, more substantial complication to the data: while muscle fibers are packed together rather tightly, there are nonetheless small gaps where multiple fibers come together. Biologically, this means there are small chambers enclosed by endomysium that are devoid of filaments and thus not considered muscle fibers. From a data perspective, this means there are small white regions within the walls that lead to small loops in the point cloud that should not contribute to the muscle fiber count. The speckling noise renders Rips persistent homology inadequate while these gap loops make it nearly impossible to choose a single optimal smoothing parameter. These are both motivations for using the persistence terrace.

To build the β_1 persistence terrace (Figure 13), we use the kernel density estimator with 100 smoothing parameter values between 2 and 40. We can identify 10-11 muscle fibers from the persistence terrace and interpret this plot in terms of size and point density of fibers. First, the largest region of overlapping terrace layers has height 9, which means at first glance that we have detected 9 of the 11 true muscle fibers. In order to detect smaller or higher density muscle fibers, we need to incorporate terrace information to the left or above this region (i.e., for smaller values of the smoothing parameter). There is a height 1 triangular region that appears around filtration value 2, the upper part of the height 9 terrace region. This suggests that there also is a high point density muscle fiber. In addition, there is a small height 10 triangular region inside the height 9 region. The small filtration value implies that the point density of the corresponding one-dimensional

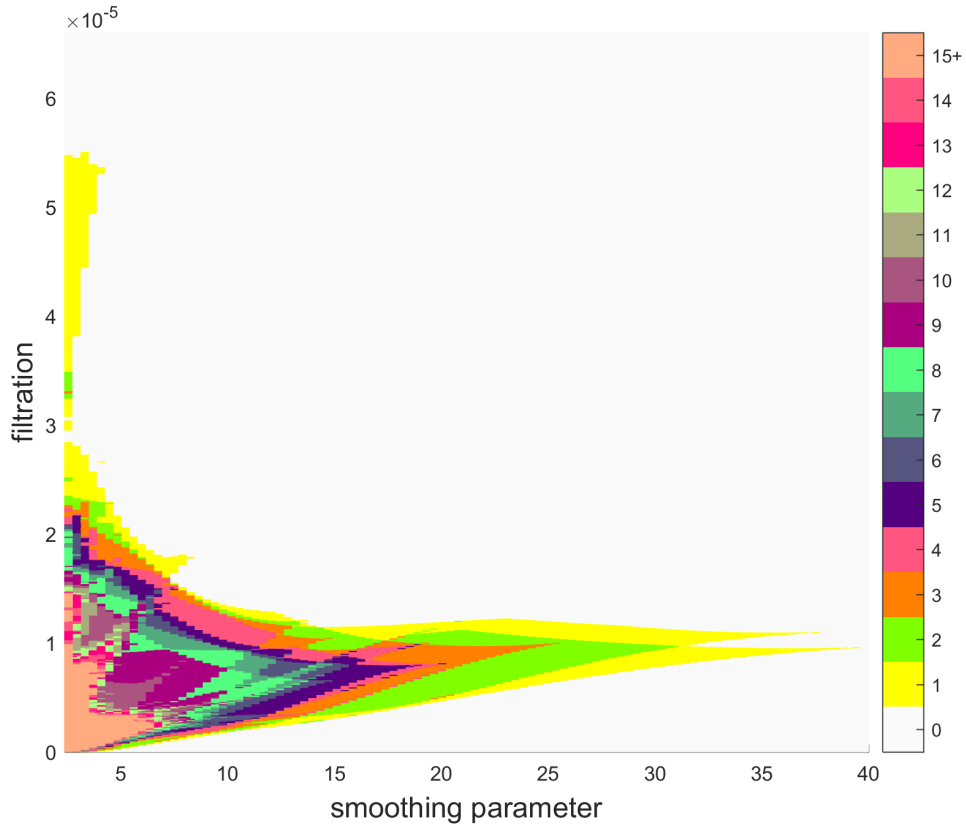


Figure 13: Satellite view of the β_1 persistence terrace computed from the 6,500 point cloud sampling of the muscle tissue cross-sectional image.

hole is not as high as others. If we include the region in counting the number of significant muscle fibers, then we find 11 muscle fibers in total.

We can also see that there is a fairly prominent vertically oriented region extending to filtration value 5.5, giving terrace heights in the range 1-3. This implies that there is a small sized but high point density one-dimensional hole. The terrace region may correspond to the muscle fiber gaps (loops in the endomysium that do not enclose any filaments). It is difficult to get a precise reading of all the gaps in Figure 12 because they are filled with noise pixels. These non-fiber loops are small in size but have comparable point density to the actual muscle fibers. Thus, they correspond to the top-left region in the persistence terrace. So while this portion of the analysis is more murky, it does seem that the persistence terrace is able to detect and count some of the muscle fiber gaps.

5 Discussion

5.1 Algorithmic Improvements

To create a persistence terrace we compute the Morse complex persistent homology for each value of the smoothing parameter specified in a pre-determined range. For large data sets, each persistent homology computation can be intensive, so multiplying by the total number of smoothing parameter values specified can be prohibitive. Fortunately, since these persistent homology computations are all independent, the procedure is readily parallelizable: just compute persistent homology for each smoothing value on separate processors then assemble. Thus, with sufficient parallel computing capability, the bottleneck for creating a persistence terrace is no worse than that of an individual persistent homology calculation (and algorithmic improvements for the latter immediately carry over to the former).

When limiting the number of available parallel processors, in order to reduce run-time one needs to reduce the number of smoothing parameter values sampled. We typically choose the range of values heuristically based on a rough estimate of the features in the point cloud one hopes to uncover, and then subdivide this range into equally sized intervals. However, a subtle question is how to choose the number of intervals: too many intervals and the computational time becomes unreasonable, too few and the persistence terrace looks coarse and becomes difficult to read. Figure 1 in Supplementary Material shows four persistence terraces computed from the data in Figure 4a, using 25, 50, 75, and 100 smoothing parameter values. An interesting topic for future research would be to develop a systematic method for determining the range of smoothing parameter values and number of intervals to subdivide it into.

5.2 Varying the Dimensions

In this paper we have focused on β_1 persistence terraces for planar point clouds. Extending from point clouds in \mathbb{R}^2 to arbitrary \mathbb{R}^n is trivial: all steps in the algorithms already allow for this possibility, as does the qualitative analysis of the resulting persistence terraces; we focused on clouds in \mathbb{R}^2 for simplicity of illustration. One can also extend from 1-dimensional topological features (i.e., loops) to any other dimension. For higher dimensions,

that is β_k with $k \geq 2$, the overall analysis should be quite similar. Most applications of TDA in the literature focus on β_1 and β_0 , so we did not explore β_2 or higher persistence terraces in this paper but one could certainly find applications. On the other hand, we tried some experiments with β_0 persistence terraces and were unable to draw any conclusions. Since β_0 is the number of connected components, the β_0 persistence terraces should encode multi-scale clustering information about the point cloud, but it is limited by the fact that clustering involves more than just point density. We will explore this point in future work.

SUPPLEMENTARY MATERIAL

Title: Algorithms and Figures (pdf)

Code for persistence terrace: R and Matlab code to generate a persistence terrace.

The package also contains all datasets used as examples in the article.

References

- Bendich, P., J. S. Marron, E. Miller, A. Pieloch, and S. Skwerer (2016). Persistent homology analysis of brain artery trees. *Annals of Applied Statistics* 10, 198–218.
- Billard, L. and E. Diday (2007). *Symbolic Data Analysis : Conceptual Statistics and Data Mining*. Hoboken, NJ: John Wiley & Sons Inc.
- Bobrowski, O., S. Mukherjee, and J. E. Taylor (2017). Topological consistency via kernel estimation. *Bernoulli* 23, 288–328.
- Bubenik, P. (2015). Statistical topological data analysis using persistence landscapes. *Journal of Machine Learning Research* 16, 77–102.
- Carlsson, G. (2009). Topology and data. *Bulletin of the American Mathematical Society* 46, 255–308.
- Chan, J. M., G. Carlsson, and R. Rabadan (2013). Topology of viral evolution. *Proceedings of the National Academy of Sciences of the United States of America* 110, 18566–18571.

- Chazal, F., D. Cohen-Steiner, and Q. Mérigot (2011). Geometric inference for probability measures. *Foundations of Computational Mathematics* 11, 733–751.
- Chazal, F., B. T. Fasy, F. Lecci, B. Michel, A. Rinaldo, and L. Wasserman (2014). Robust topological inference: Distance to a measure and kernel distance. unpublished manuscript, available at arXiv:1412.7197.
- Chazal, F., B. T. Fasy, F. Lecci, A. Rinaldo, and L. Wasserman (2015). Stochastic convergence of persistence landscapes and silhouettes. *Journal of Computational Geometry* 6, 140–161.
- Edelsbrunner, H. and J. Harer (2008). Persistent homology - a survey. *Surveys on Discrete and Computational Geometry: Twenty Years Later* 453, 257–282.
- Edelsbrunner, H. and J. Harer (2010). *Computational Topology : An Introduction*. Providence, RI: American Mathematical Society.
- Fasy, B. T., J. Kim, F. Lecci, C. Maria, V. R. T. included GUDHI is authored by Clement Maria, D. by Dmitriy Morozov, P. by Ulrich Bauer, M. Kerber, and J. Reininghaus. (2016). *TDA: Statistical Tools for Topological Data Analysis*. R package version 1.5 <https://CRAN.R-project.org/package=TDA>.
- Fasy, B. T., F. Lecci, A. Rinaldo, L. Wasserman, S. Balakrishnan, and A. Singh (2014). Confidence sets for persistence diagrams. *Annals of Statistics* 42, 2301–2339.
- Gameiro, M., Y. Hiraoka, S. Izumi, M. Kramar, K. Mischaikow, and V. Nanda (2015). A topological measurement of protein compressibility. *Japan Journal of Industrial and Applied Mathematics* 32, 1–17.
- Ghrist, R. (2008). Barcodes: The persistent topology of data. *Bulletin of the American Mathematical Society* 45, 61–75.
- Hatcher, A. (2002). *Algebraic Topology*. New York, NY: Cambridge University Press.
- Heo, G., J. Gamble, and P. T. Kim (2012). Topological analysis of variance and the maxillary complex. *Journal of the American Statistical Association* 107, 477–492.

- Lee, H., H. Kang, M. K. Chung, B. N. Kim, and D. S. Lee (2012). Persistent brain network homology from the perspective of dendrogram. *IEEE Transactions on Medical Imaging* 31, 2267–2277.
- Lum, P. Y., G. Singh, A. Lehman, T. Ishkanov, M. Vejdemo-Johansson, M. Alagappan, J. Carlsson, and G. Carlsson (2013). Extracting insights from the shape of complex data using topology. *Scientific Reports* 3, 1236. DOI: <http://dx.doi.org/10.1038/srep01236>.
- Marron, J. S. and A. M. Alonso (2014). Overview of object oriented data analysis. *Biometrical Journal* 56, 732–753.
- MATLAB (2016). *version 9.10.0 (R2016b)*. Natick, MA: The MathWorks Inc.
- Mula, J., J. D. Lee, F. Liu, L. Yang, and C. A. Peterson (2013). Automated image analysis of skeletal muscle fiber cross-sectional area. *Journal of Applied Physiology* 114, 148–155.
- Nicolau, M., A. J. Levine, and G. Carlsson (2011). Topology based data analysis identifies a subgroup of breast cancers with a unique mutational profile and excellent survival. *Proceedings of the National Academy of Sciences of the United States of America* 108, 7265–7270.
- Petri, G., P. Expert, F. Turkheimer, R. Carhart-Harris, D. Nutt, P. J. Hellyer, and F. Vaccarino (2014). Homological scaffolds of brain functional networks. *Journal of the Royal Society Interface* 11. 20140873. DOI: <http://doi.org/10.1098/rsif.2014.0873>.
- Phillips, J. M., B. Wang, and Y. Zheng (2013). Geometric inference on kernel density estimates. unpublished manuscript, available at arXiv:1307.7760.
- Ramsay, J. and B. W. Silverman (2005). *Functional Data Analysis*. New York, NY: Springer-Verlag.
- Turner, K., S. Mukherjee, and D. M. Boyer (2014). Persistent homology transform for modeling shapes and surfaces. *Information & Inference: A Journal of the IMA* 3, 310–344.
- Zomorodian, A. (2012). Topological data analysis. *Advances in Applied and Computational Topology* 70, 1–39.

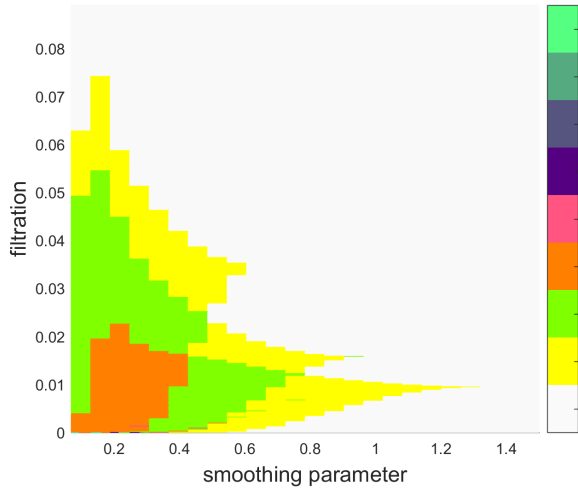
Supplementary Material

Algorithm 1 Compute Betti number values and locations from barcodes

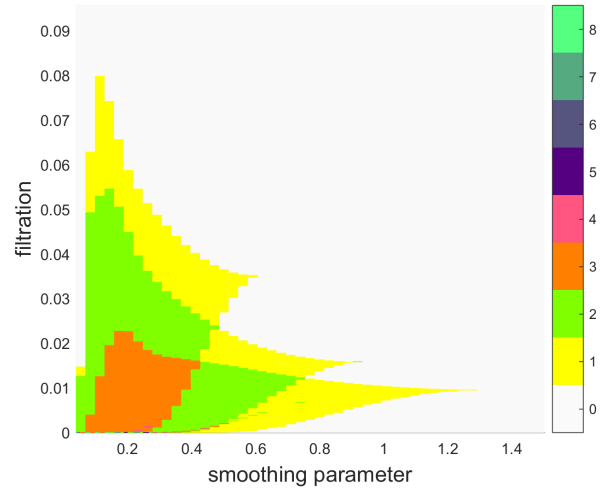
Input sp (smoothing parameter vector) and $barcodes$ (sets of barcodes)
 $kholes \leftarrow$ NULL (List of Betti number values and locations, for each smoothing parameter value)
for $i = 1 \rightarrow \text{length}(sp)$ **do**
 $kbarcode \leftarrow barcodes[[i]]\{\text{dim} = k, \text{birth}, \text{death}\}$ (Select k -dimensional barcode obtained from i th smoothing parameter value)
 $m \leftarrow$ column length of $kbarcode$ (Number of k -dimensional bars)
 if $m = 0$ (No k -dimensional bars) **then**
 $track \leftarrow \{\text{filtration}=0, \text{numk}=0\}$
 else
 $\text{filtration} \leftarrow \{\text{birth values in } kbarcode; \text{death values in } kbarcode\}$
 $\text{kBetti} \leftarrow \{\mathbf{1}_m; -\mathbf{1}_m\}$
 $track \leftarrow \{\text{filtration}, \text{kBetti}\}$ (Bind two vectors into $(2m \times 2)$ matrix, thereby assigning 1 and -1 to the birth and death points, respectively)
 Sort $track$ matrix by ‘filtration’ in ascending order
 $track\$\text{kBetti} \leftarrow \text{cumsum}(track\$\text{kBetti})$ (Replace the kBetti column by its cumulative sum)
 end if
 $kholes[[i]] \leftarrow track$
end for
return $kholes$

Algorithm 2 Compute persistence terrace matrix from Betti number values/locations

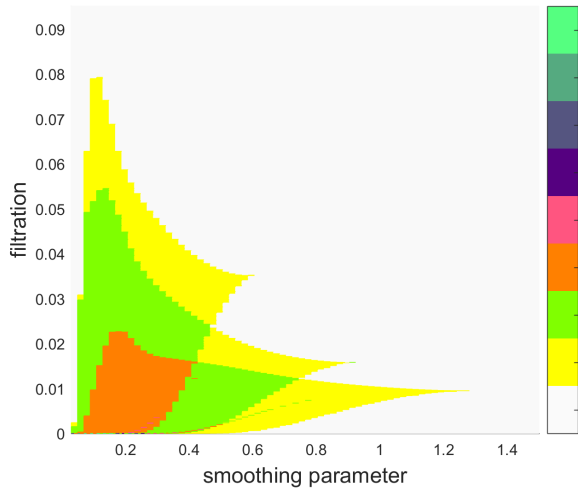
Input sp (smoothing parameter vector) and $kholes = \{ \text{filtration, } k\text{th Betti number} \}$
 $n \leftarrow \text{length}(sp)$
 $xvec \leftarrow sp$ (x values vector: smoothing parameters)
 $yvec \leftarrow \text{NULL}$ (y values vector: filtration values when the k th Betti number change)
for $i = 1 \rightarrow n$ **do**
 $yvec \leftarrow \{ yvec, kholes[[i]]\$filtration \}$ (Stack all filtration values)
end for
 $yvec \leftarrow \text{sort}(yvec)$ (Sort $yvec$ in descending order)
 $zmat \leftarrow \mathbf{0}_{\text{length}(xvec) \times \text{length}(yvec)}$ (z values matrix: k th Betti number)
for $p = 1 \rightarrow n$ **do**
 $filtration \leftarrow kholes[[p]]\$filtration$
 $kBetti \leftarrow kholes[[p]]\$kBetti$
 $zvec \leftarrow \mathbf{0}_{\text{length}(yvec)}$
 for $q = 1 \rightarrow \text{length}(kBetti)$ **do**
 $zvec = zvec + (filtration[q+1] < yvec) * (yvec \leq filtration[q]) * kBetti[q]$ (Fill out
 k th Betti numbers for all filtration values)
 end for
 $zmat[,p] \leftarrow zvec$ (Save $zvec$ to p th column of $zmat$)
end for
return $[xvec, yvec, zmat]$



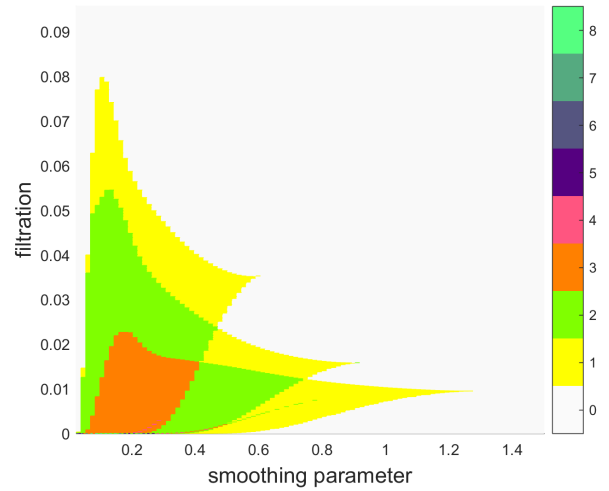
(a) 25 smoothing parameters



(b) 50 smoothing parameters



(c) 75 smoothing parameters



(d) 100 smoothing parameters

Figure 1: Resolution of persistence terrace. The online version of this figure is in color.